Int. J. Heat Mass Transfer. Vol. 23, pp. 1561–1572
Pergamon Press Ltd. 1980. Printed in Great Britain

TURBULENT STRUCTURE MEASUREMENTS IN MERCURY PIPE FLOW

L. L. EYLER* and A. SESONSKE
Purdue University, W. Lafayette, IN 47906, U.S.A.

(*Received* 20 *June* 1979 *and in revised form* 21 *April* 1980)

Abstract – Turbulent structure measurements made in fully-developed mercury ($Pr = 0.024$) pipe flow at $Re = 100\,000$ in isothermal and in nonisothermal flow subject to a constant wall heat flux of 23.3 kW m^{-2} are reported. An especially-built three-sensor hot-film probe was used to simultaneously measure the axial and radial velocity fluctuations and temperature fluctuations.

Auto- and cross-spectral densities were measured to investigate differences in heat and momentum transport in low-Prandtl number flows. Microscales were calculated. The microscale ratio of temperature to that of velocity in the axial and radial directions was found to increase significantly near the wall whereas the lateral ratio tended to decrease slightly. In all cases the temperature microscale was larger than the corresponding velocity scale. The microscale results are related to the k–ε level of turbulence modeling.

NOMENCLATURE

D, pipe diameter [m];
d_s, sensor diameter [m];
e, instantaneous fluctuating voltage [V];
$E_{xx}(kD)$, normalized autospectral density ($\equiv E_{xx}(k)/\dot{D}$);
$E_{xy}(kD)$, normalized cross-spectral density ($\equiv E_{xy}(k)/D$);
$G_{xx}(kD)$, autospectral density ($\equiv E_{xx}(kD)\cdot x^2$) [m^2 s^{-2} or °C^{-2}];
$G_{xy}(kD)$, cross-spectral density ($\equiv E_{xy}(kD)\cdot \overline{xy}$) [m^2 s^{-2} or m °C^{-1}];
k, wave number [m^{-1}]; turbulent kinetic energy [m^2 s^{-2}];
l, length scale [m];
l_s, sensor length [m];
Q_w, wall heat flux [kW m^{-2}];
r, radial pipe coordinate [m];
R, pipe radius [m];
R_ε, dissipation scale ratio;
$R_{xy}(kD)$, normalized cross-spectral correlation coefficient ($= G_{xy}(kD)/[G_{xx}(kD)G_{yy}(kD)]^{1/2}$);
S, sensitivity [V s^{-1} m or V °C^{-1}];
t, time, [s];
u, v, w, fluctuating velocity in z, r, ϕ pipe coordinate, respectively [m s^{-1}];
y, radial distance from wall [m];
z, axial pipe coordinate [m];

Greek symbols

ε, dissipation of turbulent kinetic energy [m^2 s^{-3}];
ε_θ, dissipation of turbulent temperature fluctuations [°C s^{-1}];
γ_{xy}, coherency ($\equiv G_{xy}(f)^2/[G_{xx}(f)G_{yy}(f)]$);
δ, sensor separation [m];
λ, microscale [m];
ν, kinematic viscosity [m^2 s^{-1}];
ϕ, azimuthal pipe coordinate [rad];
θ, instantaneous fluctuating temperature [°C].

Subscripts

e, energy;
u, v, axial, radial velocity;
x, y, fluctuating variable ($x, y = u, v, \theta$; $x \neq y$);
z, r, ϕ, coordinate direction;
θ, temperature;
1, 2, 3, sensor number.

INTRODUCTION

THE LACK of any universally satisfactory method for predicting turbulent transport provides an incentive for continued research [1]. Information obtained from experimental investigations can be used to further the understanding of turbulent transport mechanisms, provide for verification of existing models, and lead to the development of new ones.

In flows where turbulent transport of heat and momentum are not expected to be similar, such as in low Prandtl number fluids, it is necessary to investigate them separately. Numerous pioneering efforts, both analytical and experimental, deal with thermal transport in low Prandtl number fluids. These variously treat the problem from analytical, phenomenological, empirical, and experimental points of view and have a common goal of providing an incremental understanding to an admittedly complex problem. While

* Present address: Battelle, Pacific Northwest Laboratories, Richland, WA 99352, U.S.A.

most early works were concerned with necessarily simplified approaches, more recent analytical approaches required the advent of large digital computers before their usefulness could be most fully realized [2]. In addition, the advent of hot-film sensor measurements allowed more specific details of the turbulent fluctuation characteristics to be investigated in liquid metals.

This report describes an experimental effort with an emphasis on the statistical structure of the fluctuating variables. Reference is made to analytical work where appropriate. Mercury ($Pr = 0.024$) was the test fluid. Isothermal flow was investigated at $Re = 10^5$ and nonisothermal flow was investigated subject to a constant wall heat flux of 23.3 kW m^{-2} in a vertically oriented cylindrical pipe. These flow conditions were chosen so as to be in a regime where previously reported free convection distortion of the mean velocity and temperature profiles was minimal [3, 4].

Several reports on structure measurements in mercury pipe flow have previously been published. Flaherty *et al.* [5], presented autospectral results in mercury at $Re = 5 \times 10^4$. However, buoyancy significantly distorted the mean flow and no results were reported for fluctuating velocity structure in nonisothermal flow. In addition, no account was made for finite sensor length in determining microscales. Hochreiter [6] reported the same type of results as Flaherty *et al.* [5], at the same flow conditions in mercury but he also neglected finite sensor length effects and reported no velocity results in nonisothermal flow. Rust and Sesonske [7], Loos [8], and Caruso [9] report results of fluctuating temperature structure in mercury but did not measure velocity structure.

Significant effort has been devoted to understanding the turbulent transport structure in air flow. Bremhorst and Bulluck [10, 11] investigated the structure of heated air flow and reported cross-spectral results for both axial and radial turbulent heat transport. Bullock *et al.* [12] presented an in-depth study of narrow- and broad-band correlation coefficients in isothermal air flow. Fulachier [13] discussed spectral analogy between temperature and velocity fluctuations in a variety of wall bounded turbulent flows. Clay [14] investigated spectral analogies in water, air, and mercury flows and Lawn [18] attempted to compile a consistent picture of the turbulent transport structure in liquid metals based on an accumulation of data available to him.

In this study, fluctuation measurements were made with a specially built three-sensor hot-film probe (3SHFP) in conjunction with simultaneous measurement of mean flow using a pitot-tube and a fast response thermocouple. Details of the structure of axial and radial velocity fluctuations and temperature fluctuations were investigated using digital data analysis of the time varying response of the sensors.

Autospectral densities of the velocity fluctuations, $E_{uu}(kD)$ and $E_{vv}(kD)$, were calculated for isothermal and nonisothermal flow. These results show an indication of the effect of buoyancy on the fluctuation structure and the wave number regions where major contributions to kinetic energy occurred in these flows. The temperature autospectral density, $E_{\theta\theta}(kD)$, was similarly calculated and used to identify variations in temperature structure when compared to the velocity results. The structure of the turbulent transport terms, $\overline{uv}$ and $\overline{v\theta}$, was examined using the cross-correlation coefficients, R_{uv} and $R_{v\theta}$, the cross-spectral correlation coefficients, $R_{uv}(kD)$ and $R_{v\theta}(kD)$, and the cross-spectral densities, $E_{uv}(kD)$ and $E_{v\theta}(kD)$. As with the autospectral densities, these results indicated variations between the transport modes of momentum and heat in the flow studied.

Microscales in both isothermal and nonisothermal flows in the axial and lateral directions were calculated from measurements made in this study. Radial microscales were estimated using the results obtained by Caruso [9] in the same experimental apparatus at the same flow conditions. These results showed that the temperature microscale was consistently larger than the velocity scale in both the axial and radial directions. The ratio in these directions increased closer to the wall whereas the ratio of lateral scales showed a slight decrease near the wall.

To the authors' knowledge, the present paper is the first to present experimental cross-spectral results in a nonisothermal low-Prandtl number flow. These results are analyzed in an attempt to further the understanding of turbulent heat and momentum transport in this flow.

EXPERIMENTAL APPARATUS

Heat transfer loop

The flow system used in this study was an especially-built heat-transfer loop. The test fluid, mercury, flowed in turn through an electrically-heated test section, a circulating pump, a full-flow filter, then downward through a return section used for pressure drop measurements. The primary flow then passed through a heat exchanger where it was cooled by a secondary water loop. The secondary loop was, in turn, cooled by a chilled water supply in an adjoining laboratory.

The 132-dia. long test section ($D = 3.64$ cm) had a 65-dia. entrance length for velocity field development followed by a 67-dia. length heated with a uniform wall heat flux for thermal field development. Both the test section and return line were constructed from stainless steel pipe and were both preceded by straightening vanes to eliminate any swirl component in the flow due to passage through the pipe fittings. To insure both a true diameter and a smooth inside surface, both pipes were reamed and polished to a 0.7% variation in the inside diameter. The inside surface was hydraulically smooth to a Reynolds number of approximately 10^6 [6].

The traversing mechanism, located at the top of the heated test section, allowed three probes to be inserted into the flow 90° apart with the capability of traversing

at least 75% of the diameter. All three probes penetrated two pipe diameters upstream to minimize end effects.

Test section inlet and outlet temperatures were measured with bulk thermocouple mixing chambers which immediately preceded and followed the test section. The mercury flow rate was measured using an orifice meter and a manometer which was readable to the nearest 0.25 mm. Mercury circulation was provided by a 25 HP motor connected to the pump through a speed reducing pulley system. The pump capacity was sufficient to attain a maximum of $Re = 1.25 \times 10^5$. The filter used was a full-flow stainless steel mesh filter with a 2.5×10^{-4} mm nominal rating. Additional facility details are given by Hochreiter [6] and Eyler [3].

Instrumentation

A Thermo-Systems, Inc. (TSI), anemometry system was used in this study. Two Model 1050, constant-temperature bridges were used for velocity measurements and a Model 1040 constant current bridge was used for temperature measurements. Each of the three channels contained a Model 1057 signal conditioner which was used for filtering and amplification of sensor response signals. Voltage fluctuation signals were FM recorded on a Precision Instruments Model 6200 tape recorder. Band-pass characteristics of each channel were checked to ensure that the channels were as equivalent as possible for frequency response from 0.1 to 1000 Hz.

Mean sensor voltages were measured using a digital voltmeter after low-pass filtering to remove the fluctuating components. Fluctuation intensities were measured simultaneously using two TSI, Model 1076, true RMS meters and a TSI, Model 1060, true RMS meter at 100 s time constants. The accuracy of each RMS meter was checked against manufacturer's specifications and against each other over the frequency range 0.1 to 1000 Hz.

Hot-film probe

Two specially-built three-sensor hot-film probes (3SHFP) were used in this study in order to simultaneously measure turbulent velocities, u and v, and temperature, θ, fluctuations. The probes were manufactured by Thermo-Systems, Inc., using -20 Hg and -10 Hg type hot-film sensors. A schematic of the sensor orientation on the probes is shown in Fig. 1. The two outboard sensors (numbers 2 and 3) were oriented parallel to each other with their major axis normal to the mean flow direction and parallel to the direction of radial traverse. The central sensor (number 1) was located symmetrically between the outboard sensors with its axis in the z–r plane at a 45° angle to the mean flow direction.

In nonisothermal flow, one normal sensor was operated as a resistance thermometer with the Model 1040 temperature bridge to measure temperature fluctuations. The other normal sensor was operated in the velocity mode and responded to velocity and temperature fluctuations. The slanted sensor was operated in the velocity mode and responded to axial and radial velocity fluctuations as well as temperature

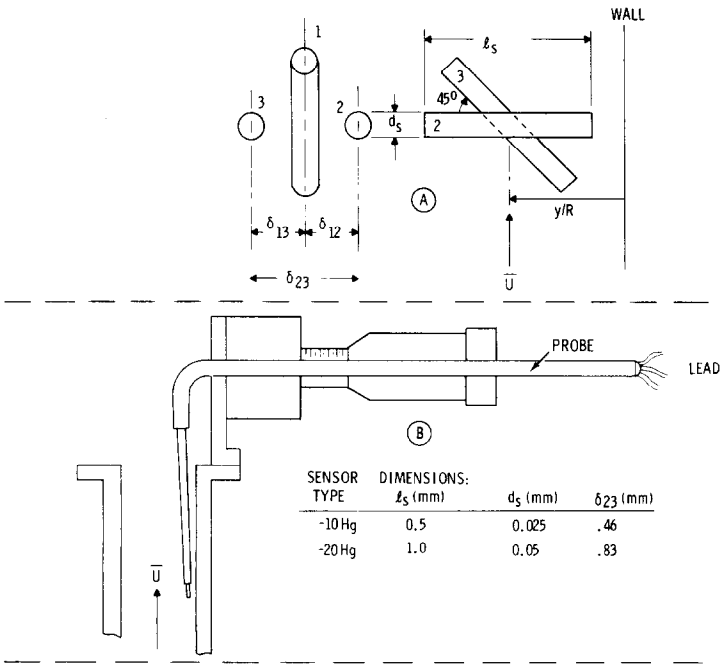

FIG. 1. Measurement probe configuration; (A) sensor geometry, (B) traversing mechanism.

fluctuations. The three response equations are

$$e_3(t) = S_{\theta,3}\theta(t), \tag{1}$$

$$e_2(t) = S_{u,2}u(t) - S_{\theta,2}\theta(t), \tag{2}$$

and

$$e_1(t) = S_{u,1}u(t) + S_{v,1}v(t) - S_{\theta,1}\theta(t). \tag{3}$$

The subscripts 1, 2, and 3 refer to sensor numbers. $S_{u,1}$ and $S_{\theta,1}$, etc., are velocity and temperature sensitivities, respectively.

Both the velocity and temperature sensitivity of the sensors were determined *in situ*. In the velocity mode, sensitivity was determined by differentiation of a power law curve-fit of mean sensor voltage drop vs velocity. Velocity calibration was performed prior to each test and rechecked during and after each test. These repeated velocity calibrations were necessary to ensure sensor calibration drift did not occur. In the temperature mode, sensitivity was determined by differentiation of a linear curve-fit of mean sensor voltage drop vs temperature. Periodic temperature calibration checks were also performed which showed the temperature sensitivity was very stable.

The FM recorded voltage responses, $e_1(t)$, $e_2(t)$, and $e_3(t)$, were replayed and digitized. The A/D convertor was a 15 bit, simultaneous sample and hold with a $\pm$ 10 V input range. The digital voltage records were stored on 1/2-in. magnetic tape for later acquisition and statistical analysis.

The data were pre-filtered before digitization using Krone–Hite 8-pole (96 db per octave) filters to remove high frequency noise in the signals. The isothermal data were filtered at 500 Hz and the nonisothermal data were filtered at 250 Hz. Above these frequencies, the response signal of the sensors was lost in background noise.

With the digital voltage records, and using equations (1)–(3), the discrete real variable time series, $u(nh)$, $v(nh)$, and $\theta(nh)$, were solved for at each discrete time, nh. These series were utilized to calculate statistical properties of the flow. Spectral analysis was conducted digitally using a Fast Fourier Transform algorithm. Each record was analyzed in 50 segments of 513 points each resulting in an estimated normalized spectral estimation error of 14%.

EXPERIMENTAL RESULTS

Autospectral densities

Isothermal and nonisothermal axial and radial velocity autospectral densities were calculated using the discrete real variable time series, $u(nh)$ and $v(nh)$, respectively. Temperature autospectral densities were calculated using $\theta(nh)$. These discrete real variable time series were obtained digitally by instantaneously solving the appropriate response equations (1)–(3). In this work, normalized autospectral results are shown on linear–log plots such that

$$\int_0^\infty kD\,E_{xx}(kD)\,\mathrm{d}\ln(kD) = 1. \tag{4}$$

Bremhorst and Bullock [10, 11] proposed that spectral plots in these coordinates are more sensitive to variations in energy containing wave-number regions than conventional log–log plots of spectra. On these linear-log plots, the area under the curves at dimensionless wave-number kD is proportional to the contribution to total energy at that wave-number, and, hence, these plots are useful in identifying wave-number regions where significant contributions to total energy exist. The regions of peak contribution can also be related to energy length scales.

The mean-square values of the fluctuating variables used to obtain normalized spectra in equation (4) were obtained directly from the real variable time series. Isothermal axial intensities obtained digitally were compared to data obtained using analog techniques and were found to be in good agreement. Similarly, digitally determined isothermal axial and radial velocity intensities were found to be in good agreement with previously published data for air and mercury pipe flow. Temperature intensities were also compared to previously reported mercury data and found to be in good agreement over most of the turbulent core. Near the wall where measured temperature intensities were less than previous mercury data, the present -10 Hg sensor provided better spatial resolution and frequency response [3].

No previous data have been reported for nonisothermal velocity intensities in mercury pipe flow. Within experimental error, data measured in this work were found to agree with the isothermal values. Thus, no buoyancy effects on nonisothermal intensity data were observed. This is consistent with the flow conditions of this work being in a range where mean flow is not significantly affected by buoyancy as previously mentioned. However, even though the nonisothermal intensity data were unaffected by buoyancy, the wave-number dependent structure is affected by buoyancy as noted subsequently.

In Fig. 2, the nomalized isothermal axial and radial velocity autospectral densities measured in this work at three radial locations are shown for $Re = 10^5$. A comparison of the centerline results of Lawn and White [15] is also shown in the figure. The axial velocity results indicate a decrease in the span of wave-numbers contributing to the total axial energy, $\overline{u^2}$, as the wall is approached. The wave-number of the peak contribution appears to decrease as the wall is approached. This trend is in agreement with that of the air results of Bremhorst and Bullock [10] and Lawn and White [15]. This trend, corresponding to an increased peak energy containing length scale as the wall is approached, indicates the existence of the large-scale fluctuations being generated near the wall and their eventual degradation to smaller scale structure in the turbulent core.

The radial velocity autospectral density results in

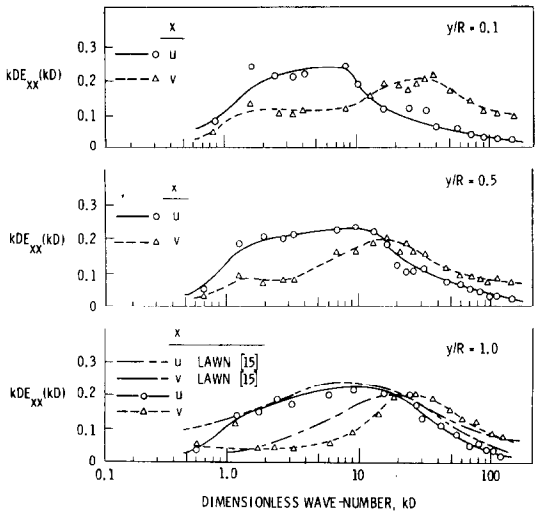

FIG. 2. Radial variation of isothermal axial and radial velocity autospectral density at $Re = 1 \times 10^5$.

Fig. 2 indicate the occurrence of the peak contributing components of the flow at higher wave-numbers than evident in the axial velocity autospectral densities. These results are also consistent with other isothermal radial spectral data [11, 15].

Several observations are evident from the non-isothermal spectra shown in Fig. 3. Perhaps the most significant is the difference between the nonisothermal velocity spectra and the isothermal velocity spectra shown in Fig. 2. The experimental results indicate that the span of wave-numbers making the major contribution to the total energy is much less than was seen in the isothermal autospectral density results. It is also evident that the magnitude of the peak contribution is greater and more sharply defined than in the isothermal case. The length scale corresponding to the peak contribution to axial energy tends to decrease as the wall is approached.

Heating effects on velocity autospectral density have been noted by Bremhorst and Bullock [11] and by Lawn and White [15] for heated air flow in a pipe, although no previous results have been reported for low-Prandtl number fluids. Bremhorst and Bullock observed a shifting effect on their radial velocity autospectral density. The shifting was towards lower wave-numbers and amounted to nearly a factor of 2 shift of the peak contribution to radial energy. In a previous work, Bremhorst and Bullock [10] mentioned only that the structure was virtually identical for isothermal and nonisothermal axial velocity fluctuations.

The difference observed in the present isothermal and nonisothermal autospectral density results may be due to density gradient effects which exist across individual eddy structures. While Launder [16] and Lumley *et al.* [17] have approached the problem of gravitational effects on turbulent transport applied to stably stratified atmospheric shear flows, added com-

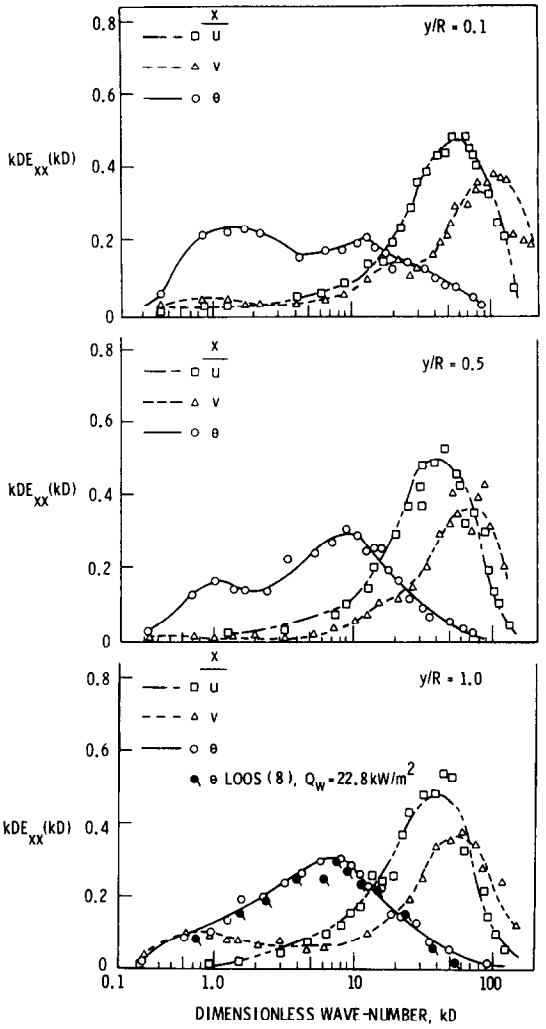

FIG. 3. Radial variation of nonisothermal velocity and temperature autospectral density at $Re = 1 \times 10^5$ and $Q_w = 23.3\ \mathrm{kW\ m^{-2}}$.

plications due to wall effects, such as appear in the pressure–velocity correlations [2], are not well understood. Consequently, at this time a confirmed explanation for the magnitude and direction of the wave-number shifting is currently lacking. It should also be noted that the previously mentioned work of Lawn [18] did not include any buoyancy effects in compiling a structural description of liquid metal flows.

The temperature autospectral densities are also shown in Fig. 3. These data were obtained simultaneously with the measurements from which the nonisothermal velocity spectra were calculated. For comparison, Loos' [8] temperature autospectral density results at the centerline are also shown and are seen to be in very good agreement with the present data.

Comparison of the temperature autospectral density with the nonisothermal velocity autospectral density in Fig. 3 shows very little similarity in structure. It is observed that the peak contribution to

temperature energy occurs at much lower wave-numbers than the peak contributions to velocity energy. It is interesting to note the existence of the large peak that occurs in the temperature autospectral density near the wall and its disappearance in the centerline spectra. Bremhorst and Bullock [10, 11] found a similar low wave-number peak in their air results. They found this second peak in both their velocity and temperature data and attempted to explain it in terms of large-scale generations which occur near the wall and maintain structure a significant downstream distance and into the core region.

Coherency and points measurements

The turbulent transport terms, $\rho\overline{uv}$ and $\rho c_p\overline{v\theta}$, which occur in the Reynolds equations written and reduced to the pipe flow geometry being studied, have physical significance when measured at a point. Multiple sensor probes which are often used to measure these turbulent fluxes and their structure characteristically require the compensation for measured fluctuations at one sensor with response measured at another sensor. Since sensors must be physically separated on multiple sensor probes, it is necessary to determine the adequacy of the compensation by verifying that the probe typifies a point measurement. This is true of X-probes as well as other sensor configurations. In the present study, point approximation was verified up to $kl_s \simeq 1.0$ by determining the coherency between pairs of sensors on the 3SHFP. Both velocity and temperature coherency was measured.

The coherency between two random fluctuating signals is interpreted to be a measure of the degree of correlation between the two signals. Coherency is defined as

$$\gamma^2_{xy}(f) = \frac{G^2_{xy}(f)}{G_{xx}(f)G_{yy}(f)} \tag{5}$$

where $G_{xy}(f)$ is the frequency cross-spectral density between signals $x(t)$ and $y(t)$ while $G_{xx}(f)$ and $G_{yy}(f)$ are the autospectral densities, respectively. By definition, $0 \leq \gamma^2_{xy}(f) \leq 1$. Thus for $\gamma^2_{xy}(f) = 1$, the signals are perfectly correlated and hence, in terms of turbulent fluctuations, over frequency (or corresponding wave-number) ranges where $\gamma^2_{xy}(f) = 1$, the probe can be expected to typify a point response.

Figure 4 shows the temperature coherency between parallel -10 Hg sensors (0.51 × 0.25 mm) and -20 Hg sensors (1.0 × 0.05 mm) on the two 3SHFPs used. Data at two radial locations are shown for $Re = 10^5$ and $Q_w = 23.3\ \mathrm{kW\ m^{-2}}$. The coherency between the smaller (-10 Hg) sensors at the smaller separation distance is higher at all wave-numbers than the larger (-20 Hg) sensors.

Figure 5 shows the coherency between the same parallel sensors responding to axial velocity fluctuations. For comparison, temperature coherency is also shown in Fig. 5. The temperature coherency and the velocity coherency of the smaller -10 Hg sensors

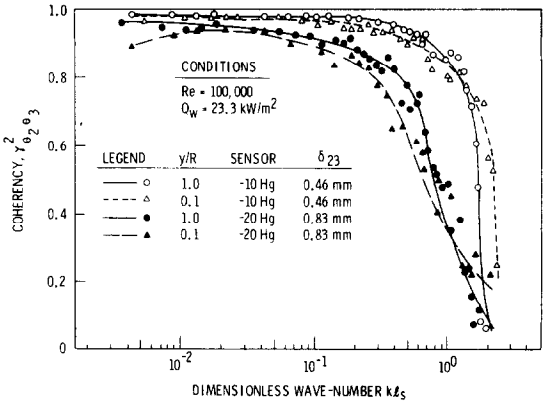

FIG. 4. Coherency between -10 Hg and -20 Hg temperature sensors at $Re = 1 \times 10^5$.

is very nearly the same at all wave-numbers. This is an indication that the -10 Hg 3SHFP very closely approximates a point response up to $kl_s \approx 1.0$. The coherency between the -20 Hg sensors is not as high nor does it extend to as high wave-numbers as the -10 Hg coherency. An explanation for the disagreement between the -20 Hg temperature and velocity coherency is lacking. All the results presented in this paper were obtained with the response data of the smaller -10 Hg sensors.

In Figs. 4 and 5, it is apparent that the coherency decreases rapidly above $kl_s = 1.0$. This observation indicates that one sensor does not adequately compensate for response at an adjacent sensor at higher wave-numbers. Hence, caution must be exercised in interpreting cross-spectral data at wave-numbers beyond $kl_s = 1.0$.

While the data shown in Figs. 4 and 5 are plotted vs kl_s, it must be recognized that the sensor separation distance, δ_{23}, may also affect the upper wave-number limit for a highly coherent response. On the -10 Hg 3SHFP, the two outboard parallel sensors were separated a distance ($\delta_{23} = 0.46$ mm) very nearly the same

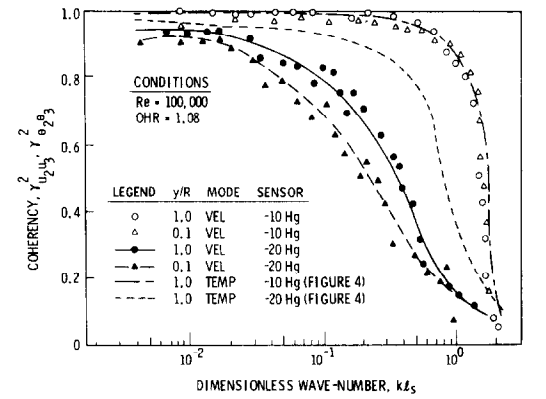

FIG. 5. Coherency between -10 Hg and -20 Hg velocity sensors at $Re = 1 \times 10^5$.

as the sensor length (l_s = 0.51 mm). Hence we were unable to determine which dimension is the most severely restricting. It was found, though, that when all three sensors on the 3SHFP were operated in the temperature mode and the coherence between each pair was plotted on the same kl_s axis, there were no distinguishable differences in the rolloff characteristics of the coherency between any pair [3].

This work is not the first to recognize that the use of the response multiple sensor probes to typify point measurements may be severely complicated by the effects of finite sensor separation distance. Several papers have been published on this effect (see, for example, Wyngaard [19]) and corrective approximations have been proposed and applied. However, the applicability of the proposed corrective approximations to high wave-number response and subsequently derived spectral statistics is dependent upon the manner in which sensor response data are reduced. In the present work, available corrective approximations were determined to be of no particular value in relation to the data reduction techniques used. Hence, the actual limitations of the multiple sensor probe used in this work were determined *in situ* and spectral statistics are viewed accordingly.

Previous results have also been reported that indicate hot-film sensor response may be seriously degraded in both amplitude and phase lag when operated at high overheats in highly conducting fluids such as mercury [20]. However, for the conditions studied in this work, these effects were determined to be negligible [3].

Cross-spectral densities

Isothermal and nonisothermal cross-spectral densities were determined from discrete real variable time series. The normalized results are shown in Figs. 6 and 7 and correspond to the same data from which corresponding autospectral density results were obtained. By definition, the normalized cross-spectral correlations at a given wave-number represent a proportionality to the total transport. Wave-number regions of significant transport are readily identified when nomalized cross-spectral density results are plotted on a linear–log plot subject to

$$\int_0^\infty kD\, E_{xy}(kD)\, \mathrm{dln}(kD) = 1. \qquad (6)$$

The centerline results in Figs. 6 and 7 are unnormalized cross-spectral densities, $G_{uv}(kD)$ and $G_{v\theta}(kD)$. The finite, nonzero areas under these centerline results correspond to the nonzero total correlations, R_{uv} and $R_{v\theta}$, respectively. The fact that the net cross products are nonzero at the centerline is a result of the inability to completely separate the axial and radial velocity components at the centerline using the present measurement techniques. At the other radial locations, the separation of the variables was shown to be adequate [3].

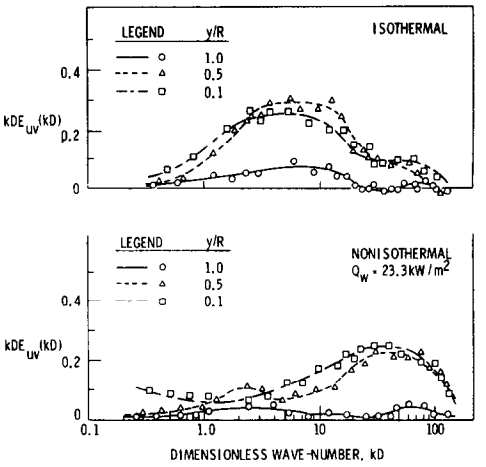

FIG. 6. Radial variation of isothermal and nonisothermal velocity cross-spectral density at $Re = 1 \times 10^5$.

It is apparent in Fig. 6 that, as with the autospectral densities, there is a significant difference between the isothermal and nonisothermal structure. This shifting of the maximum is nearly an order of magnitude and the range of major contributing wave-numbers is lessened in the case of nonisothermal results. These trends follow the autospectral density results very closely.

The cross-spectral density results between radial velocity fluctuations and temperature fluctuations shown in Fig. 7 exhibit the combined effects of the velocity and temperature structure. The range of peak contributing wave-numbers is, in general, below that for the nonisothermal velocity cross-spectra previously discussed. It is also evident that significant contributions are made in the pipe diameter length scale range as exhibited by the lesser peak near $kD \simeq 1$. This corresponds to the large scales associated with the lesser peak of the temperature fluctuations shown in Fig. 3.

This comparison between $E_{uv}(kD)$ and $E_{v\theta}(kD)$ obtained from simultaneous measurements in the flow further evidences dissimilarities in heat and momentum transport in low-Prandtl number fluids. Heat transport seems to be more locally centered in wave-number structure than does momentum transport.

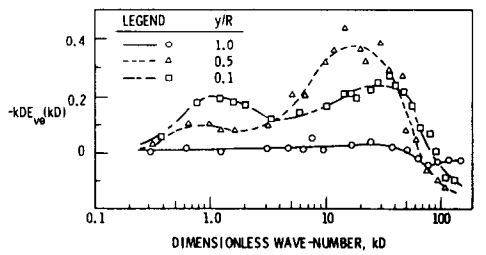

FIG. 7. Radial variation of velocity–temperature cross-spectral density at $Re = 1 \times 10^5$ and $Q_w = 23.3\,\mathrm{kW\,m^{-2}}$.

One tractable explanation is due directly to a Prandtl number effect. As Prandtl number decreases below unity, the relative effect of increased thermal conductivity even on a microscale level results in a 'smearing' of the temperature field thus leading to large temperature length scales in relation to velocity scales. This point is further evidenced in microscale results presented below. When coupled to production, diffusion, and dissipation of the turbulent fluxes, this leads to increased net transport of thermal energy occurring in lower wave-number regions.

In further support of this contention, cross-spectral correlation coefficients were also calculated from the present data. This coefficient, defined as

$$R_{xy}(kD) = \frac{|G_{xy}(kD)|}{[G_{xx}(kD)G_{yy}(kD)]^{1/2}} \tag{7}$$

represents an efficiency of transport at a given wave-number. In the lower wave-number, large length scale region, the cross-spectral correlation of equation (7) indicated that thermal energy is transported much more efficiently than is momentum at similar wave-numbers [3]. This, again may be due to a direct consequence of the smearing effect of thermal conductivity on the structure of the temperature field.

Microscales

In this work, axial velocity and temperature microscales were calculated using the response of hot-film sensors oriented normal to the mean flow direction. Lawn [21] found by dimensional reasoning that axial velocity microscales should scale as

$$\frac{\lambda_{z,u}}{R} = C(y/R)(R^+)^{-1/2} \tag{8}$$

where $C(y/R)$ is a radially dependent scaling factor and R^+, defined as RU^*/ν, is a function of Reynolds number. Using the second moment of spectra method and raw autospectral densities, calculated microscales were found to be factors of 2–3 larger than given by Lawn's scaling of equation (8). Further discussion of this difference is noteworthy as it typifies an inherent error in many microscale measurements.

The second moment method for determining microscales involves integration of the energy spectra as [21]

$$\frac{2}{\lambda_{z,u}^2} = \int_0^\infty k^2 E_{uu}(k)\mathrm{d}k. \tag{9}$$

This can be rearranged and normalized to yield

$$\frac{\lambda_{z,u}}{D} = \frac{1}{D}\left[\frac{2}{\int_0^\infty k^2 E_{uu}(k)\mathrm{d}k}\right]^{1/2}. \tag{10}$$

For sensors which are longer than the smallest structure of the flow, length attenuation can occur [19] which results in the integral in equation (10) converging too rapidly. This leads directly to an over estimation of the microscale. A correction scheme was developed to account for this effect in calculating both velocity and temperature microscales. The scheme involved evaluating the integral in parts. Measured spectra were used over the portion of wave-numbers unaffected by length attenuation and assumed wave-number laws over the remaining wave-number region. This procedure was not unlike that developed by Clay [14] to determine dissipation in the flows he studied. Corrected isothermal results, shown in Fig. 8, were found to be in very good agreement with Lawn's proposed scaling and his air flow results.

Using the correction scheme, microscales of axial velocity and temperature fluctuations were calculated. These results are presented in Fig. 9 as a function of radial position for $Re = 10^5$. The isothermal velocity microscale is seen to increase with radial position towards the centerline. A similar observation is evident for the nonisothermal velocity microscale and the temperature microscale.

The nonisothermal velocity microscale results indicate a radial variation very similar to that of the isothermal results although they are less in magnitude. This appears to be consistent with the previously discussed variation in the velocity autospectral density, at least as the nonisothermal velocity autospectral density was shifted to higher wave-numbers. However, it should be noted that aspects of the correction scheme were not readily verifiable when applied to nonisothermal data [3] as assumed high wave-number spectral distributions have not been investigated sufficiently. Hence, the nonisothermal velocity microscales are subject to less confidence than are the isothermal results.

In Fig. 10 the ratio of the axial velocity microscale and the axial temperature microscale are shown for $Re = 10^5$. Considering the isothermal velocity microscales, it is interesting to note the agreement between the raw data microscale ratio and the ratio calculated using the corrected results as shown in Fig. 10. Both ratios are in good agreement in magnitude and in radial trend. This observation indicates that the sensor

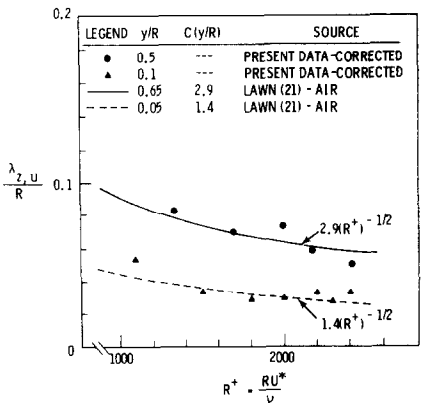

FIG. 8. Reynolds number dependence of axial velocity microscales in isothermal flow.

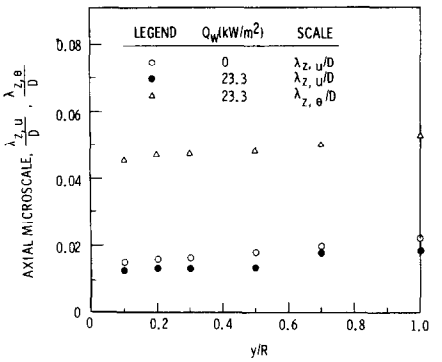

FIG. 9. Comparison of axial velocity and temperature microscales at $Re = 1 \times 10^5$ ($R^+ = 4.8 \times 10^3$).

response attenuation due to the finite length has a similar effect on the integral of the second moment of both the velocity and temperature autospectra. Further, it is observed that the isothermal ratio exhibits an increase as the wall is approached. In terms of eddies, this radial trend in the microscale ratio indicates that perhaps a higher conduction effect occurs near the wall where a larger temperature gradient exists, thus causing an increase in the size of temperature eddies with respect to velocity eddies.

Radial velocity and temperature microscales were measured only at the centerline in this study. A two-point spatial correlation method was used [3, 21]. The isothermal centerline microscale, $\lambda_{r,u}$, was in good agreement with the data of Lawn [21]. The centerline temperature scale, $\lambda_{r,\theta}$, was approximately 60% larger than that calculated from Caruso's data [5]. This difference is felt to be a direct consequence of the larger sensors which he used. He used spatially separated -20 Hg sensors and, as noted previously, these larger sensors do not respond equally well when separated only one sensor length.

Nevertheless, by making the assumption that a uniform schematic error existed in Caruso's data due to sensor size and separation, a variation with radial position can be inferred from his data. Using the present centerline value as a reference in conjunction with Lawn's [21] radial velocity microscales, the ratio of radial microscales can be determined. The results, shown in Fig. 11 indicate a fairly uniform ratio in the turbulent core region with a marked increase near the wall.

As a further indication of the anisotropic eddy structure, lateral microscales were calculated at $Re = 10^5$. Lateral velocity scales were calculated only for isothermal flow while temperature scales were calculated in nonisothermal flow with $Q_w = 23.3\ \text{kW m}^{-2}$. The results of the calculations for the lateral microscales are shown in Fig. 12 for three runs at the same flow conditions. The ratio of the microscales is also shown. The agreement of the scales for the three runs is an indication of the reproducibility of the data.

As with the axial and radial microscales, the present lateral results indicate the temperature scale to be larger than the velocity scale. However, this ratio of lateral scales indicates a decrease in the relative size of dissipating temperature eddies to dissipating velocity eddies as the wall is approached. This is an opposite trend from the axial and radial microscale ratios. Since no mean temperature or velocity gradient exists in the azimuthal direction in pipe flow, the variation in the lateral microscale ratio may be interpreted directly as a measure of the conduction effect that exists on a microscale level across individual eddies.

In addition to these microscale results, the following inference about energy containing length scales can be made from the spectral data. From Fig. 3, the energy length scale of axial velocity fluctuation, l_e^u, is approximately 0.025 D at the centerline. The energy length scale of temperature fluctuations, l_e^θ, is approximately 0.15 D at the centerline. It is interesting to note that $l_e^\theta \simeq l_e^u/0.17$ which is close to $l_e^\theta = l_e^u/\sqrt{Pr} = l_e^u/0.15$. Also, in Fig. 3 it can be seen that the ratio of l_e^θ/l_e^u is very nearly constant for all three radial locations shown. Furthermore, Hochreiter [6] showed that Kudva's [22] ethylene glycol ($Pr = 70$) velocity and temperature energy length scales were approximately related as $l_e^\theta \simeq l_e^u/5.0$ which is not very different from $l_e^\theta = l_e^u/\sqrt{Pr} = l_e^u/8.3$. Lawn's [21] air results indicate $l_e^\theta \simeq$

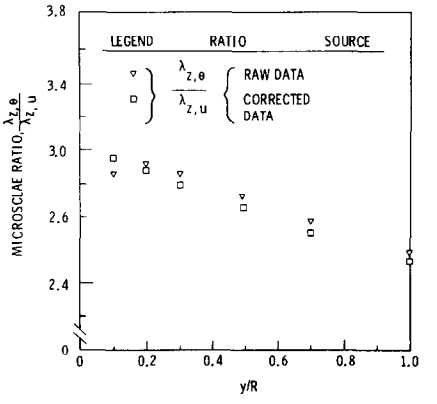

FIG. 10. Comparison of ratio of the raw and corrected axial velocity and temperature microscales at $Re = 1 \times 10^5$.

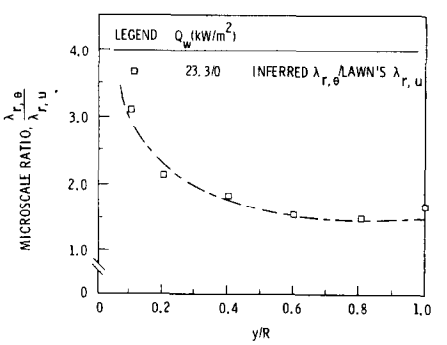

FIG. 11. Radial microscale ratio at $Re = 1 \times 10^5$.

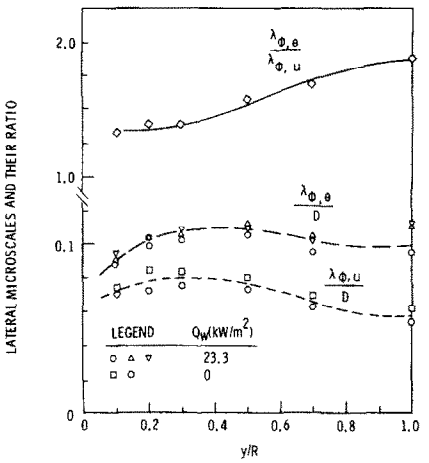

FIG. 12. Lateral microscales and their ratio at $Re = 1 \times 10^5$.

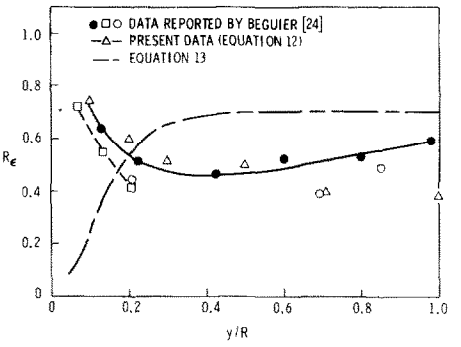

FIG. 13. Dissipation time scale ratio.

$l_e^u/0.7$ which is likewise not very different from $l_e^\theta = l_e^u/\sqrt{Pr} = l_e^u/0.84$.

These observations lend support to the temperature and velocity energy length scales being related as the reciprocal of the square root of Prandtl number. The interesting aspect of this observation is that the conduction effect on the principal contribution to total energy is dependent on Prandtl number, even in the strongly anisotropic low wave-number regions, in a manner similar to that proposed for isotropic flow.

The microscale results discussed above have been found useful in modeling turbulent dissipation of temperature energy at the k–ε level of turbulent transport modeling [23] of mercury pipe flow. They should also be useful in the more general ASM model proposed by Sha and Launder [2] for application to liquid metal flows.

In the modeled transport equation for temperature fluctuations (see for example [1, 24]), it is necessary to either solve an additional transport equation for the dissipation of the temperature fluctuations, ε_θ, or model it directly. The latter method assumes that the dissipation of temperature energy can be related to dissipation of kinetic energy ε. The quantity relating them is the ratio of dissipation time scales or

$$R_\varepsilon = \frac{\varepsilon \overline{\theta^2}}{\varepsilon_\theta q^2}. \tag{11}$$

Beguier *et al.* [24] showed that equation (11) can be determined from microscale and fluctuation data when rewritten as

$$R_\varepsilon = 5\, Pr \frac{\overline{u^2}}{q^2}\left(\frac{\lambda_\theta}{\lambda_u}\right)^2. \tag{12}$$

Results calculated using equation (12) are shown in Fig. 13 along with the data presented by Beguier *et al.* [24] for flow in a heated pipe. The present data show a trend towards an asymptotic value of about 0.4 near the centerline with a higher ratio of nearly 0.8 near the wall. This trend is in very good agreement with other data presented by Beguier *et al.* [24], but is in disagreement with the emprical expression

$$R_\varepsilon = 0.7\,(1 - e^{-Pe_t/70})^2 \tag{13}$$

proposed by Sha and Launder [2] for low-Prandtl number flow. In equation (13), Pe_t is the turbulent Peclet number defined as $(k^2/\nu\varepsilon)Pr$.

However, it should be noted that some concern has been raised as to whether the dissipation time scale ratio given by equation (11) (and hence (12)) is indeed an appropriate way to model dissipation of temperature fluctuations. If velocity and temperature fluctuations are in equilibrium, then the time scale ratio R_ε should be given by the ratio of their decay rates. However, Warhaft and Lumley [25] performed an extensive evaluation of temperature decay rate and concluded that there was no evidence in their work to indicate that an equilibrium value of R_ε existed in wind tunnel experiments. They concluded also that the ramifications of this conclusion may well extend to other shear flows wherein the value of R_ε may well depend upon more than just local values of relative scale size of velocity and temperature fields.

CONCLUSIONS

An especially built three-sensor hot-film probe was used to simultaneously measure turbulent axial and radial velocity components and temperature fluctuations. Data obtained in this work were presented to elicit differences in the structure of momentum and heat transfer in low-Prandtl number fluid flow.

Autospectral density results depicted not only the structure differences between velocity and temperature but also the significant buoyancy effects on velocity spectral structure in heated flow. Although significant buoyancy effects have been documented for mean flow structure in mercury flows, the observed shift in energy spectrum to higher wave-numbers in the heated flow has been heretofore unreported. In previous liquid metal work, velocity structure in heated flows was not measured due to inability to isolate velocity response of hot-film sensors in mercury flow.

Cross-spectral density results also showed a marked difference in the isothermal versus nonisothermal structure of the $\overline{uv}$ velocity correlation. Data for cross-spectral density of $\overline{v\theta}$ showed that contributions to turbulent transport of heat is spread between length scales of the order of the pipe diameter and $0.02D$ with a maximum occurring near $0.05\,D$.

Calculated microscale results were found to be in good agreement with a Reynolds number variation proposed by Lawn [21] after accounting for finite sensor length attenuation. Ratios of the temperature to the velocity microscale showed that the temperature size was as much as three times the velocity size in both the axial and radial directions and only slightly larger in the lateral direction. These trends evidence the anisotropies of the scale lengths. The microscale results have been used with some success to model the dissipation of temperature fluctuations through a dissipation time scale ratio even though it must be recognized that an equilibrium dissipation time scale ratio may not exist for many flows.

Acknowledgement—The financial assistance of the National Science Foundation (Grant GK-35776) is gratefully acknowledged.

REFEENCES

1. J. L. Lumley, in *Prediction Methods for Turbulent Flows*, D. Olivari, Course Director, Von Karman Institute for Fluid Dynamics, Lecture Series 76 (3–7 March 1975).
2. W. T. Sha and B. E. Launder, A general model for turbulent momentum and heat transport in liquid metals, Argonne National Laboratory, ANL–77–78 (November 1977).
3. L. L. Eyler, Turbulent structure measurements and transport modeling in liquid metals, Ph.D. Thesis, Purdue University (1978).
4. A. Sesonske, L. L. Eyler and G. Klein, Effect of free convection on turbulent flow mercury heat transfer, *Trans. Am. Nucl. Soc.* **21,** 410–411 (1975).
5. T. W. Flaherty, L. L. Eyler and A. Sesonske, Turbulent structure measurements in nonisothermal mercury pipe flow, in *Proceedings of the Third Symposium on Turbulence in Liquids*. Rolla, Missouri (1975).
6. L. E. Hochrieter, Turbulent structure of isothermal and nonisothermal liquid metal pipe flow, *Int. J. Heat Mass Transfer* **17,** 113–121 (1974).
7. J. H. Rust and A. Sesonske, Turbulent temperature fluctuations in mercury and ethylene glycol in pipe flow, *Int. J. Heat Mass Transfer* **9,** 215–221 (1969).
8. R. L. Loos, Characteristics of turbulent temperature fluctuations in mercury, M.S. Thesis, Purdue University (1971).
9. S. Caruso, Space-time correlations of temperature in turbulent mercury pipe flows, M.S. Thesis, Purdue University (1977).
10. K. Bremhorst and K. J. Bullock, Spectral measurements of temperature and longitudinal velocity fluctuations in fully developed pipe flow, *Int. J. Heat Mass Transfer* **13,** 1313–1329 (1970).
11. K. Bremhorst and K. J. Bullock, Spectral measurements of turbulent heat and momentum transport in fully developed pipe flow, *Int. J. Heat Mass Transfer* **13,** 2141–2154 (1973).
12. J. J. Bullock, R. E. Cooper and F. H. Abernathy, Structure similarity in radial correlations and spectra of longitudinal velocity fluctuations in pipe flow, *J. Fluid Mech.* **88(3)** 585–608 (1978).
13. L. Fulachier, Spectral analogy between temperature and velocity fluctuations in various turbulent flows, ASME paper, Heat Transfer Division, 78–HT–2 (1978).
14. J. P. Clay, Turbulent mixing of temperature in water, air, and mercury, Ph.D. Thesis, Univ. of California, San Diego (1973).
15. C. J. Lawn and R. S. White, The turbulent structure of heated pipe flow, CEGB Report RD/B/N2150 (1972).
16. B. E. Launder, On the effects of a gravitational field on the turbulent transport of heat and momentum, *J. Fluid Mech.* **67(3),** 569–581 (1975).
17. J. L. Lumley, O. Zeman and J. Siess, The influence of buoyancy on turbulent transport, *J. Fluid Mech.* **84(3),** 581–597 (1978).
18. C. J. Lawn, Turbulent temperature fluctuations in liquid metals, *Int. J. Heat Mass Transfer* **20,** 1035–1044 (1977).
19. J. C. Wyngaard, Spatial resolution of the vorticity meter and other hot-wire arrays, *J. Scient. Instrum.* **2,** 983–992 (1969).
20. C. A. Sliecher and G. B. Lim, Measurement of unsteady flows in mercury with hot-film anemometers, in *Proceedings of the Third Symposium on Turbulence in Liquids*. Rolla, Missouri (1975).
21. C. J. Lawn, The determination of the rate of dissipation in turbulent pipe flow, *J. Fluid Mech.* **48(3),** 477–505 (1971).
22. A. K. Kudva, The structure of turbulent velocity and temperature fields in ethylene glycol flowing in a pipe at low Reynolds numbers, Ph.D. Thesis, Purdue University (1970).
23. L. L. Eyler, unpublished, Battelle, Pacific Northwest Laboratories (1978).
24. C. Beguier, I. DeKeysen and B. E. Launder, Ratio of scalar and velocity dissipation time scales in shear flow turbulence, *Physics Fluids* **21(3),** 307–310 (1978).
25. Z. Warhaft and J. L. Lumley, An experimental study of the decay of temperature fluctuations in grid-generated turbulence, *J. Fluid Mech.* **88(4),** 659–684 (1978).

MESURES SUR LA STRUCTURE DE LA TURBULENCE

Résumé—Des mesures sur la structure de la turbulence sont faites pour un écoulement établi de mercure ($Pr = 0,024$) dans un tube à $Re = 100\,000$, soit isotherme, soit soumis à une condition de flux pariétal constant égal à $23{,}3\,\mathrm{kW \cdot m^{-2}}$. On utilise une sonde triple à fils chauds spécialement conçue pour mesurer simultanément les fluctuations de vitesses axiale et radiale et les fluctuations de température. Des densités spectrales sont mesurées pour analyser les différences entre les transports de chaleur et de quantité de mouvement aux faibles nombres de Prandtl. On calcule des microéchelles. Le rapport de la microéchelle de température à celle de la vitesse dans les directions axiale et radiale augmente significativement près de la paroi, tandis que le rapport latéral tend à décroître légèrement. Dans tous les cas la microéchelle de température est plus grande que celle des vitesses. Les résultats sont reliés au niveau de turbulence du modèle $k - \varepsilon$.

MESSUNGEN DER TURBULENZ-STRUKTUR IN DER ROHRSTRÖMUNG VON QUECKSILBER

Zusammenfassung—Es wird über Messungen der Turbulenzstruktur in der Rohrströmung von Quecksilber ($Pr = 0{,}024$) bei $Re = 100\,000$ in isothermer und nichtisothermer Strömung bei einer konstanten Wärmestromdichte an der Wand von 23,3 kW/m^2 berichtet. Eine eigens entwickelte Dreifachsensor-Heißfilm-Sonde wurde zur gleichzeitigen Messung der axialen und radialen Geschwindigkeits- und Temperatur-Schwankungen verwendet. Um Unterschiede beim Wärme- und Impulstransport in Strömungen bei kleiner Prandtl-Zahl zu untersuchen, wurden die Auto- und die Kreuz-Spektral-Dichte gemessen. "Microscales" wurden berechnet. Es wurde gefunden, daß das Verhältnis der "Microscales" von Temperatur zu Geschwindigkeit in axialer und in radialer Richtung nahe der Wand beträchtlich zunimmt, wohingegen das laterale Verhältnis dazu neigt, leicht abzunehmen. In allen Fällen waren die "Microscales" der Temperatur größer als die der Geschwindigkeit. Die "Microscale"-Ergebnisse werden auf das k–ε-Niveau des Turbulenz-Modells bezogen.

ИЗМЕРЕНИЕ СТРУКТУРЫ ТУРБУЛЕНТНОСТИ ПРИ ТЕЧЕНИИ РТУТИ В ТРУБЕ

Аннотация — Проведены измерения турбулентной структуры при полностью развитом ($Pr = 0{,}024$) изотермическом и неизотермическом течениях ртути в трубе при $Re = 100\,000$ и постоянной плотности теплового потока на стенке, равной 23,3 квт/м$^{-2}$. Для одновременного измерения аксиальных и радиальных пульсаций скорости и флуктуаций температуры использовался специально сконструированный пленочный термоэлемент с тремя датчиками. Были проведены измерения скоростных и взаимных спектральных плотностей для выяснения различий в процессах переноса тепла и импульса в потоках с малым числом Прандтля. Микромасштабы определялись расчетным путем. Найдено, что отношение микромасштаба температур к продольному и поперечному масштабу скорости значительно возрастает у стенки, в то время как эти отношения поперек потока несколько уменьшаются. Во всех случаях микромасштаб температуры превышал соответствующий микромасштаб скорости. Полученные результаты предназначены для моделирования теплопереноса при неоднородной турбулентности с помощью моделей второго порядка.